MRU Cardington Technical Note No. 17

Evaluation of turbulent wind measurements by different instruments

by

A.L.M. Grant

12 February 1991

Met. Office Research Unit
RAF Cardington
Shortstown
Beds, MK42 0TH

MRU CARDINGTON

Note

This paper has not been published and PMetO(Cardington) should be consulted before quoting from it.

MRU Cardington Technical Note No. 17

Evaluation of turbulent wind measurements by different instruments

by

A.L.M. Grant

12 February 1991

Met. Office Research Unit
RAF Cardington
Shortstown
Beds, MK42 0TH

Note

This paper has not been published and PMetO(Cardington) should be consulted before quoting from it.

Evaluation of turbulent wind measurements by different instruments

A.L.M Grant

12 February 1991

1 Introduction

Micrometeorological studies often require accurate measurements of the vector wind with high temporal resolution. Such measurements are more difficult to make than might appear at first sight because the presence of the instrument and support structures, such as masts, can disturb the air flow causing significant errors in turbulent statistics. Because it is difficult to calculate the flow around a complex three dimensional shape the accuracy of an instrument must usually be determined empirically through wind tunnel studies and/or comparison with other instruments in the atmosphere.

This paper describes comparisons between several different instruments, including a recently developed sonic anemometer that is available commercially.

2 Instrumentation and processing

Three anemometers, a Kaijo-Denki sonic anemometer-thermometer, a Gill Instruments sonic anemometer and a non-orthogonal propeller array, were mounted on three, six meter, guyed cylindrical masts. Adjacent masts were separated by nine meters. On each day when data were to be collected the masts were straightened (as judged by sighting up the mast), made vertical and rotated so that the anemometers faced approximately into the mean wind. Measurements on the bottom mast sections showed them to be vertical to within 1/2°, while wind inclinations determined from the sonic anemometers were mostly less than 1° (with a maximum value of 1·6°). When necessary adjustments were made to the masts between runs to keep the anemometers facing into wind.

The analogue outputs from the Kaijo-Denki sonic and the propeller array were logged by a MicroVax II computer using a 12 bit analogue to digital converter at a sample rate of 20·776 Hz. The individual channels of the A/D converter were calibrated using a precision voltage supply. The Gill Instruments sonic provides both digital and analogue outputs. The digital outputs are used in this study and these were logged through a serial port. The data rate in this case was 20·831 Hz. The two logging programs ran independently but were synchronized at the start by using the event flag facility provided by the VMS operating system of the MicroVax.

Turbulence statistics and spectra were calculated from the processed timeseries after applying rotations to make the mean lateral and vertical wind components zero and the removal of a linear trend from each of the wind components. The spectra and cospectra

were calculated using an FFT routine and the spectral estimates block averaged over frequency to produce ten smoothed estimates per decade. No corrections have been made for the different recording rates of the analogue and digital signals so that statistics calculated from the Kaijo-Denki sonic and propellers are for a slightly different period to those from the Gill Instruments sonic (the difference amounts to about 5 seconds in a 1500 second run).

A brief description of each of the anemometers will be given now.

2.1 Kaijo-Denki sonic anemometer

This is the reference instrument for this study. The model used was a Kaijo-Denki DAT 300 sonic anemometer-thermometer with a type TR61A head. In this type of head the three transducer pairs are arranged to measure wind components along two horizontal paths separated by 120° and a single vertically oriented path. A significant source of error that can occur with this arrangement of paths arises from wakes generated by the transducers (Wyngaard and Zhang 1985, Grant and Watkins 1989), but errors can be minimised by keeping the anemometer pointed so that the wind direction is within about $20 - 30°$ of the axis of symmetry. The orientation of the Kaijo-Denki sonic was checked frequently to ensure it was always pointing into wind.

The Kaijo-Denki processing unit outputs analogue voltages proportional to the wind components along the transducer paths. These voltages were converted to speeds using the factory calibration and orthogonal wind components calculated.

2.2 Gill Instruments sonic anemometer

In the Gill Instrument sonic the transducer paths are inclined by 45° to the horizontal to minimize the effects of transducer shadowing on the wind measurements. During this intercomparison the sonic was oriented so that the wind direction did not coincide with any of the transducer pairs or with the support struts. Because of this no information is available on the variation of errors with wind direction.

The Gill sonic provides a digital output over an RS232 serial line and analogue output which is synthesized from the digital data. Only the digital data are used in this study. Orthogonal wind components are calculated by the microprocessor in the sonic head unit from the measured non-orthogonal components, so subsequent processing consists only of sorting the serial data and correcting for occasional losses (only 3 blocks of 20 records had to be replaced in the whole dataset).

The wind components obtained from the Gill sonic anemometer are also 'corrected' for the effects of flow disturbance by the head. The corrections are derived from a wind tunnel study of windspeed errors as a function of wind direction. In the version of the anemometer used here all three wind components are corrected using the same factor (for the orientation used in this study the correction is about 2%). Later versions of the anemometer apply separate corrections to the vertical component.

2.3 Gill propeller anemometers

It has been suggested that the Kaijo-Denki sonic maybe subject to random calibration drifts over long periods (Kraan and Oost 1989), so as an independent check a

non-orthogonal array of propeller anemometers was also deployed during this intercomparison. The propeller anemometers are of interest in themselves since they are frequently used in micrometeorological studies. The array consists of three propeller anemometers arranged around a cone with a horizontal axis and an opening angle of 60°. This geometry ensures that there is a significant wind component along the axis of all three anemometers so there is little likelyhood of any of the propellers stalling, except in light winds. The propellers used had a diameter of 19cm and were made of polystyrene. The three anemometers were individually calibrated in a wind tunnel before the comparison.

During processing corrections have been applied to the propeller data to account for the non-cosine response and the limited frequency response. The frequency response correction assumes that the propellers behave as a first order linear system with a length constant of 0·7m for axial flow. This value of the length constant gives a good inertial subrange in the vertical velocity spectra and is close to the manufacturers value of 0·8m for this type of propeller.

3 Sampling errors

All measured turbulence quantities suffer from statistical sampling error due to finite averaging times and in any comparison there will be a certain amount of scatter due to this. For an averaging time T, the statistical uncertainty in a single variance measurement is,

$$\epsilon^2 = \frac{4\tau}{T}$$

where τ is the integral timescale. For a covariance measurement the uncertainty is,

$$\epsilon^2 = \frac{2\tau}{T}\left(1 + \frac{1}{r^2}\right)$$

where r is the correlation coefficient between the variables. The above results assume that $T >> \tau$ and that the timeseries are Gaussian.

In the present data the spectra of the horizontal wind components do not, in general, have a well defined peak (see figure 1), so that an integral timescale cannot be determined to calculate the expected uncertainty in the variances. For the vertical wind component, however, there is a clear spectral peak with a wavelength of 25m. With an average windspeed of $7ms^{-1}$ this implies an integral timescale of 0·6 seconds ($\tau = \frac{\lambda_{max}}{2\pi U}$, where λ_{max} is the wavelength of the spectral peak and U is the mean windspeed). For averaging time of 1500 seconds the statistical uncertainty in σ_w should be approximately 4% and if statistically independent measurements from two different instruments are compared the rms difference will be approximately 6%. For the present data the correlation coefficient between u and w is 0·27 and the integral timescale, estimated from stress spectra, is about 1 second. This suggests an uncertainty of 15% for a single stress estimate and an rms difference between independent measurements of approximately 20%. For an intercomparison instruments are usually sited close together so that statistics from different instruments will generally not be independent. This correlation between measurements will lead to smaller rms differences than calculated above.

The statistical uncertainty in integral quantities is also reflected in the comparisons between spectra. Power spectral estimates derived from a Gaussian timeseries follow

a χ^2 distribution with two degrees of freedom, and consequently the relative error in any spectral estimate is one (e.g. Bendat and Piersol 1971). The power spectra to be presented were obtained from the original Fourier transform by averaging over frequency bands with a constant width on a logarithmic scale. Since the original Fourier estimates have a fixed frequency interval the final spectrum is more heavily smoothed at high frequencies, so the uncertainty in the smoothed spectral estimates will decrease with increasing frequency. Consequently the scatter in the ratio between spectra obtained from different instruments should also decrease with increasing frequency. For sufficiently low frequencies (i.e. long wavelengths) fluctuations measured by different instruments are likely to be correlated, which will tend to reduce the variability in the spectral ratios. The variability should, therefore, be a maximum at some intermediate frequency.

4 Results

Figure 1 show the averaged normalised spectra of the three wind components from the Kaijo-Denki. Individual spectra have been normalised by the vertical velocity variance. The spectra show that the energy in horizontal wind components is associated with large wavelengths, while the energy in the vertical velocity component is concentrated at smaller wavelengths. There is a suggestion that at small wavelengths the v and w spectra fall of rather more rapidly than $k^{-2/3}$ which might be a result of response limitations in the Kaijo-Denki sonic anemometer.

4.1 Mean Windspeeds

Mean windspeeds from the Gill sonic and propeller anemometers are compared with the Kaijo-Denki windspeeds in Figures 2a and b respectively. Both the Gill sonic and the propellers underestimate the windspeed by about 2% relative to the Kaijo-Denki. The accuracies given by the manufacturers are 1% for the Kaijo-Denki and 1·5% for the Gill sonic, so that the observed difference between the two sonic anemometers is within the quoted accuracies. However, the agreement between the Gill sonic and the propellers suggests that there is a small calibration error in the Kaijo-Denki.

4.2 Velocity component variances

Figures 3a and 3b show the comparison of the variance of the longitudinal wind component, σ_u^2, from the Gill sonic and propeller anemometers respectively against the Kaijo-Denki. The variances from both the Gill sonic and propeller anemometers are approximately 6% smaller than the corresponding Kaijo-Denki values. This is similar to what would be expected if the results of the windspeed comparison are taken to indicate a 2% calibration error in the Kaijo-Denki. For the propeller array there might also be a small under estimate due to limited response.

Figures 4a and 4b show the comparisons for the variance of the lateral velocity component, σ_v^2. The Gill sonic variances are approximately 9% lower than the Kaijo-Denki values whilst the propeller variances are about 9% larger than the Kaijo-Denki. Part of the difference between the Kaijo-Denki and Gill sonic might be caused by the suspected calibration error, which would leave a residual underestimate of about 5%.

In the case of the propeller data allowing for an error in the Kaijo-Denki makes the comparison worse. The value of σ_v^2 obtained from the propeller anemometers is sensitive to the correction for non-cosine response that is applied during processing although the variance of the longitudinal wind component, σ_u^2, is not. Therefore, while errors in this correction would not affect σ_u^2 to seriously they could produce relatively large errors in σ_v^2. This might explain why the propeller values of σ_v^2 are larger than the Kaijo-Denki values while the propeller u variances agree quite well with the Kaijo-Denki values.

Figures 5a and 5b show the comparisons for the variance of the vertical velocity component, σ_w^2. The agreement between the Gill sonic and the Kaijo-Denki variances is poor, the Gill sonic variances are about 30% smaller than the Kaijo-Denki variances, although despite this difference in magnitude, the correlation between the variances from the two anemometers is good. In contrast the propeller variances are in good agreement with the Kaijo-Denki data. This good agreement is a consequence of the correction for limited frequency response that is applied to the propeller data, since for the height where the comparison was carried out the peak in the w spectrum is only just resolved by the uncorrected data. The scatter in Figures 5a and b is consistent with that calculated above in Section 3.

4.3 Shear stress

Figures 6a and 6b show the comparisons for the longitudinal shear stress component $\overline{uw}$. The Gill sonic gives stress estimates that are 17% smaller than the corresponding Kaijo Denki estimates. This difference is consistent with the results obtained above with the vertical velocity variances, if it is assumed that the error in the vertical velocity is simply a scaling error and is not associated with significant crosstalk between different wind components.

The propeller shear stresses are also smaller than the Kaijo-Denki values, in this case by about 12%. This is somewhat larger than would be expected from the results of the variance comparison given above. However, a simple error analysis shows that shear stresses measured by the propeller array used here are rather sensitive to differential errors in the propeller calibrations. For example a 1% error in the calibration of the top propeller can lead to an 8% error in the shear stress, and an apparent wind inclination of about $0 \cdot 7°$. If a co-ordinate rotation is performed to make $\overline{w} = 0$ the error in the shear stress is reduced to between 2-3%. The present propeller data show a persistent wind inclination of about 2°, which is substantially larger than that from either the Kaijo-Denki or Gill sonics. Such an apparent wind inclination could arise from an error in the calibration of the top propeller of about 3% which would result in a 10% error in the shear stress, after the co-ordinate transformation. The error in the windspeed would only be about 1%. The true source of this error in the propeller shear stresses is not known but the above shows how a relatively small calibration error can lead to a significant error in the shear stress.

The scatter in both the Gill sonic and propeller comparisons is similar to that calculated above in section 3.

5 Spectral Comparisons

Comparisons between spectra highlight errors that are frequency or wavelength dependent, such as response errors, noise or problems at specific frequencies due, for example, to mechanical resonances. The effect that such errors might have on integral statistics will depend on the spectral distribution of the turbulence kinetic energy.

5.1 Gill sonic

Figures 7a and 7b show ratios between spectra measured by the Gill sonic and the Kaijo-Denki for the horizontal wind components u and v respectively. For wavenumbers (in these and subsequent plots wavenumber=1/wavelength) less than $0 \cdot 1m^{-1}$ the spectral ratios are independent of wavenumber and slightly less than one for both u and v. The values of the ratios are consistent with the results from the variance comparisons. For wavenumbers greater than $0 \cdot 1m^{-1}$ the Gill sonic u spectrum becomes progressively smaller than the Kaijo-Denki spectrum, while the ratio between the v spectra remains constant to the largest wavenumbers resolved. The response of a sonic anemometer can be complex, being determined by a combination of line averaging, path separation, the flow field itself etc. so interpretation of Figures 7a and b in terms of the response of one of the anemometers is difficult. Some further insight can be gained by considering the quantity $\frac{k^{2/3}kS(k)}{\sigma^2}$ which is shown in Figure 8a for the u spectrum. For the Kaijo-Denki $\frac{k^{2/3}kS(k)}{\sigma^2}$ approaches a constant value and shows no tendency to decrease at larger wavenumbers. This is consistent with the u spectrum having an inertial subrange at large wavenumbers. With the Gill sonic there is a clear decrease for wavenumbers greater than $0 \cdot 1m^{-1}$. This indicates that the spectrum is falling off faster than $k^{-2/3}$, presumably due to the effects of limited response. Hence, in Figure 7a, the decrease in the spectral ratios at large wavenumbers reflects the response of the Gill sonic. Figure 8b shows $\frac{k^{2/3}kS(k)}{\sigma^2}$ for the lateral wind component. In this case both the Kaijo-Denki and Gill sonics show a decrease at the smallest wavelengths, suggesting that the spectral ratio is constant in Figure 7b because the two anemometers have similar responses and not because they are capable of resolving high frequency fluctuations in the lateral wind component. The relative behaviour of the Kaijo-Denki u and v spectra at large wavenumbers is consistent with response calculations that have been done for this transducer geometry (Kaimal et al 1968, Horst 1973).

Figure 9 shows the ratio between the vertical velocity spectra obtained by the Gill sonic and Kaijo-Denki. There is a distinct bias in the ratios that is independent of wavenumber and in magnitude is consistent with the results of the variance comparison above. Compared with the Figures 7a and 7b the variability in the spectral ratios on wavenumber for vertical velocity is very large at small wavenumbers, which is not expected from the discussion in Section 3. above. This is probably due to the effect of instrumental tilt, since at small wavenumbers $kS_{ww}(k) << kS_{uu}(k)$ or $kS_{vv}(k)$ so that the w spectrum will be very sensitive to small instrumental tilts. The procedure used to correct for instrumental tilt, i.e forcing $\overline{w} = 0$, can only detect the component of the tilt that is along the direction of the mean wind, any component of the tilt that lies across the mean wind direction cannot be detected or corrected in this way. However, since very little of the total variance is contributed by small wavenumbers the effect on σ_w^2 is negligible.

Unlike power spectra, cospectra can be positive or negative so it is not appropriate to use ratios to compare them. However, if differences are used then some form of weighting is required to ensure that the overall difference is not dominated by a few cases with very large stresses. For this reason cospectra have been normalised to the Kaijo-Denki stress before differencing. The results are shown in Figure 10. The difference shows a small negative bias indicating that the Kaijo-Denki cospectrum is slightly larger than the Gill sonic cospectrum, which is consistent with the stress comparison shown above. The maximum difference occurs around the cospectral peak. This is seen more clearly in Figure 11 were the average difference between the Gill sonic and Kaijo-Denki cospectra is shown together with the average Kaijo-Denki cospectrum. The shapes are clearly very similar, which would be expected if the difference in shear stress is due to a sensitivity error in one or other of the wind components.

5.2 Propellers

The propeller results are basically similar to those presented above for the Gill sonic, except of course the average cospectral ratios are consistent with the Kaijo-Denki, propeller comparisons given above. Figures 12a and b show the results for the horizontal wind components. The propeller u spectra show a loss of signal for wavenumbers greater than about $0 \cdot 05m^{-1}$, which is consistent with the propeller array having an effective length constant of 0·7m for fluctuations in the longitudinal wind component. The ratios for the lateral wind component, in contrast, show no corresponding decrease, so for the lateral wind component the propeller array appears to have a similar response to the Kaijo-Denki. These results emphasise that it is not possible to characterise the response of a vector wind instrument by a single length constant.

6 Discussion

The main intention of this paper was to assess the performance of the Gill Instruments sonic anemometer which has recently become available. An independent check on the Kaijo-Denki sonic was provided by an array of propeller anemometers which are also commonly used in micrometeorological studies. Propeller anemometers are relatively cheap, compared to sonic anemometers, robust and have stable calibrations. Being mechanical they have disadvantages compared to sonic anemometers, in particular higher starting speeds and the possibility of slow mechanical degradation which may be difficult to detect. However, the present comparisons show that provided corrections for non-cosine and frequency response errors are made propeller anemometers can provide turbulence measurements to an accuracy of about 10%.

The Gill sonic showed good agreement with the Kaijo-Denki for windspeed and the horizontal velocity variances, although the Gill sonic may underestimate σ_v^2 by about 5% relative to the Kaijo-Denki. In contrast, the vertical velocity variances from the Gill sonic were approximately 30% smaller than corresponding Kaijo-Denki variances. The propeller data indicate that the error is associated with the Gill sonic rather than the Kaijo-Denki. Additional evidence for an error in the Gill sonic vertical velocity measurements can be obtained by considering the ratio $\frac{kS_{ww}}{kS_{uu}}$, which is shown in Figure 13. For wavenumbers in the inertial subrange part of the spectrum this ratio should tend to a constant value of $\frac{4}{3}$, which occurs with the Kaijo-Denki spectra for wavenumbers

between 0·05 and $0 \cdot 1m^{-1}$ (although strictly the turbulence cannot be isotropic at these wavelengths). At greater wavenumbers the ratio decreases because of the difference response for the vertical and longitudinal wind components noted above. With the Gill sonic the $\frac{4}{3}$ ratio is not approached within the bandwidth of the data, and although the ratio increases for wavenumbers greater than $0 \cdot 1m^{-1}$ this is due to the different responses for fluctuations in the longitudinal and vertical wind components.

Instrument comparisons cannot readily identify the source of errors such as the underestimate of σ_w^2 by the Gill sonic that has been observed here. However, the fact that the horizontal wind components are not as seriously affected as the vertical component suggests that the problem does not lie in the measurement of the original non-orthogonal wind components. It seems more likely that flow distortion by the sonic head itself is responsible. The head geometry used by the Gill sonic is intended to reduce the effects of transducer shadowing errors on turbulence measurements, and other sonic anemometers with the same geometry are available. One such is the TR61B head manufactured by Kaijo-Denki. Whilst this head has the same geometry as the Gill sonic, it is considerably larger and has differently shaped transducers. The signal processing, however, is similar to that of the TR61A head, except that orthogonal wind components are output rather than the components along the transducer paths. Comparisons have been carried out between a TR61A head and a TR61B head. These comparisons were made at 20m with the TR61B head kept in a fixed orientation and the TR61A head rotated to keep it pointed into the mean wind as before. Data processing details were the same as above.

Figure 14. shows the ratio between the vertical velocity variances measured by the TR61B head and the TR61A head as a function of wind direction relative to the TR61B head. The TR61B vertical velocity variances are between 15 and 30% smaller than the TR61A values, and although there are only a few data available the difference appears to depend on the incident wind direction. A similar dependence was not seen with the Gill sonic because the orientation of the head relative to the mean wind direction was kept fixed. As with the Gill sonic the ratio $\frac{kS_{ww}(k)}{kS_{uu}(k)}$ indicates that it is the TR61B variances which are in error.

The errors in vertical velocity from a TR61B head appear to be similar to those of the Gill sonic but the error in the variance of the lateral wind is different. The Gill sonic appears to underestimate σ_v^2 by about 5% but with TR61B head σ_v^2 appears to be overestimated by 5-10%. Possibly the error in the vertical velocity is due to flow blockage by the transducer arrangement while the error in the lateral wind component might be mainly due to transducer shadowing errors, which will be quite different for the two sonic anemometers because of the differently shaped transducers.

Mortensen et al (1988) have developed a correction for the TR61B head based on wind tunnel studies. These corrections can be applied in real time or during subsequent data processing. Similar corrections are clearly required for the Gill sonic anemometer. Corrections derived from wind tunnel studies are applied to the Gill sonic measurements in real time. However, the correction to the horizontal components are the same and based on scalar windspeed measurements, while the correction for the vertical component is based on only a single wind inclination (note that with the anemometer used in this study the same correction is applied to all three wind components). It is not clear that these corrections are adequate for high quality turbulence measurements, but if a correction scheme similar to that of Mortensen et al could be developed the Gill anemometer should be able to provide high quality turbulence data.

It should be clear from this study that turbulence statistics can be affected in complex ways by instrumental errors. In particular the simplest measure of the error in an anemometer, the error in the mean windspeed, is not, in general, a very good indicator of the possible errors that might occur in higher order moments.

7 References

Bendat, J. S. and Piersol, A. G.,1971: Random data: analysis and measurement procedures. New York (John Wiley and Son Inc).

Grant, A. L. M. and Watkins, R. D., 1989: Errors in turbulence measurements with a sonic anemometer. Boundary-Layer Meteorol., 46, 181-194.

Horst, T. W, 1973: Spectral transfer functions for a three component sonic anemometer. J. Appl. Meteor., 12, 1072-1075.

Kaimal, J. C., Wyngaard, J. C. and Haugen, D. A., 1968: Deriving power spectra from a three component sonic anemometer. J. Appl. Meteor., 7, 827-837.

Kraan, C. and Oost, W. A., 1989: A new way of anemometer calibration and its application to a sonic anemometer. J. Atmos. Oceanic Technol., 6, 516-524.

Mortensen, N. G., et al: 1986: Two-years-worth of turbulence data recorded by a sonic anemometer data aquisition system. In 6th symposium of meteorological observations and instrumentation, Jan 12-16, 393-396.

Wyngaard, J. C. and Zhang, Z. F., 1985: Transducer shadow effects on turbulence spectra measured by sonic anemometers. J Atmos. Oceanic Technol., 2, 548-558.

8 Figure legends

Figure 1. Average spectra obtained with the Kaijo-Denki sonic anemometer. Before averaging the spectra were normalised by the vertical velocity variance. Full line: longitudinal wind component u, Dotted line: lateral wind component v, Dashed line: vertical wind component w.

Figure 2. Comparison between mean windspeeds measured by (a) the Gill sonic and Kaijo-Denki, (b) the propeller array and the Kaijo-Denki. The full line marks perfect agreement. The dashed line is a least squares fit through the origin.

Figure 3. Comparison between the variances of the longitudinal wind component measured by (a) the Gill sonic and Kaijo-Denki, (b) the propeller array and Kaijo-Denki. The full line shows perfect agreement. The dashed line is a least squares fit through the origin.

Figure 4. Comparison between the variances of the lateral wind component measured by (a) the Gill sonic and Kaijo-Denki, (b) the propeller array and Kaijo-Denki. The full line shows perfect agreement. The dashed line is a least squares fit through the origin.

Figure 5. Comparison between the variances of the vertical velocity wind component measured by (a) the Gill sonic and Kaijo-Denki, (b) the propeller array and the Kaijo-Denki. The full line shows perfect agreement. The dashed line is a least squares fit through the origin. The dotted lines show the rms scatter expected for independent measurements of the variance.

Figure 6. Comparison between the longitudinal shear stress component measured by (a) the Gill sonic and Kaijo-Denki, (b) the propeller array and the Kaijo-Denki. The full line shows perfect agreement. The dashed line is a least squares fit through the origin. The dotted lines show the rms scatter expected for independent measurements of the shear stress.

Figure 7. Ratio between Gill sonic and Kaijo-Denki spectra. (a) Longitudinal wind component. (b) lateral wind component.

Figure 8. $\frac{k^{2/3}kS(k)}{\sigma.^2}$ for the longitudinal wind component (a) and the lateral wind component (b). The full line shows the result for the Kaijo-Denki spectra the dashed line the results for the Gill sonic.

Figure 9. Ratio between the Gill sonic and Kaijo-Denki vertical velocity spectra.

Figure 10. Difference between the Gill sonic and Kaijo-Denki stress cospectra. The individual stress cospectra have been normalised to the Kaijo-Denki shear stress.

Figure 11. Averaged difference between the normalised Gill sonic and Kaijo-Denki stress cospectra (full curve). The dashed curve shows the averaged normalised Kaijo-Denki stress cospectrum (multiplied by 0.17).

Figure 12. Ratio between propeller and Kaijo-Denki spectra. (a) Longitudinal wind component. (b) lateral wind component.

Figure 13. Ratio between the vertical velocity and longitudinal velocity component spectra for the Kaijo-Denki sonic (full curve) and the Gill sonic (dashed curve).

Figure 14. Ratio between vertical velocity variances measured by the TR61B and TR61A Kaijo-Denki probe heads as a function of wind direction relative to the TR61B head.

nS(n)
10+00
10-01
10-02
10-03
10-05
10-04
10-03
10-02
10-01
10+00
Wavenumber

Figure 1

Figure 2

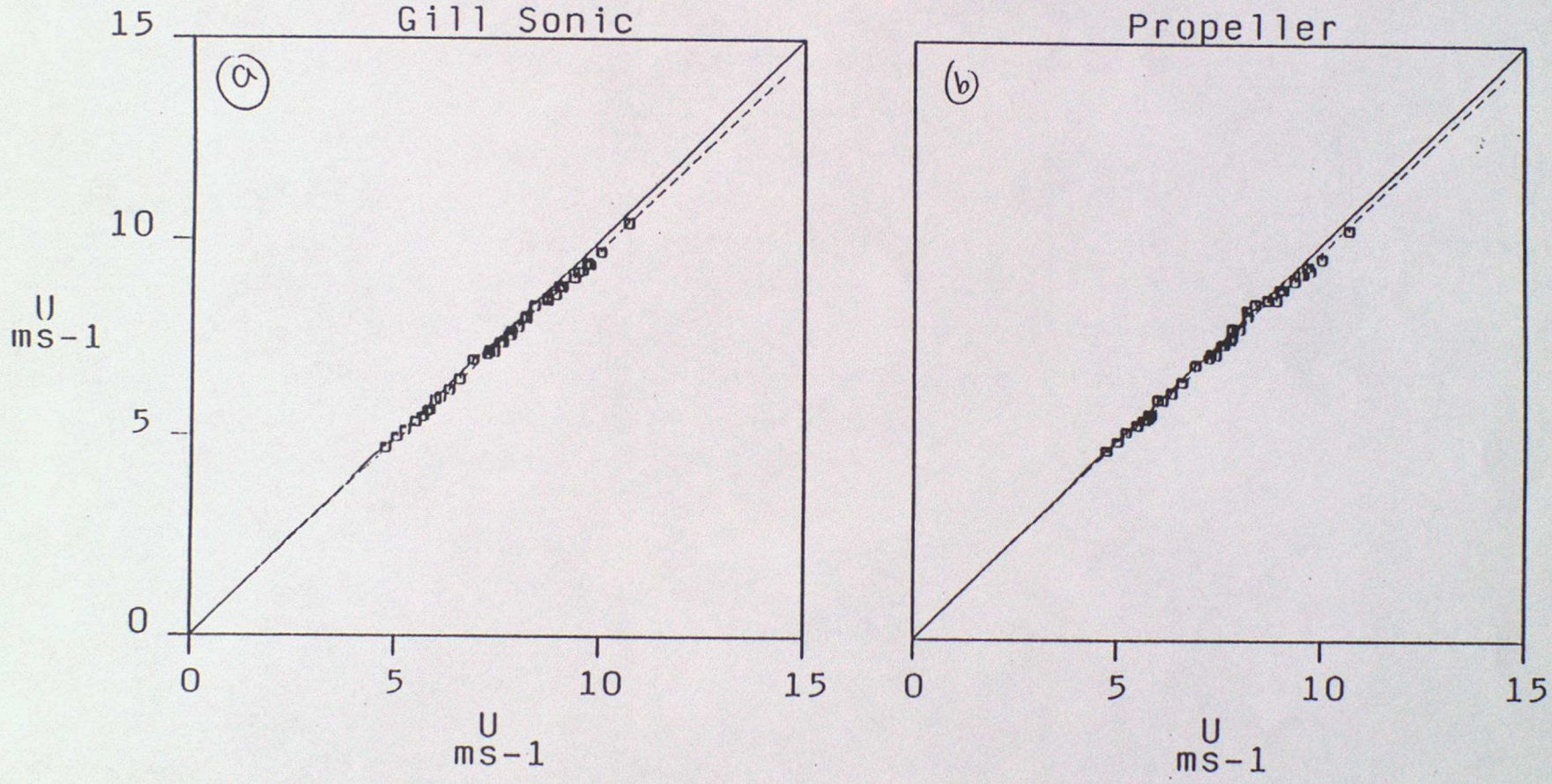
Gill Sonic
(a)
15
10
5
0
U
ms-1
0
5
10
15
U
ms-1
Propeller
(b)
0
5
10
15
U
ms-1

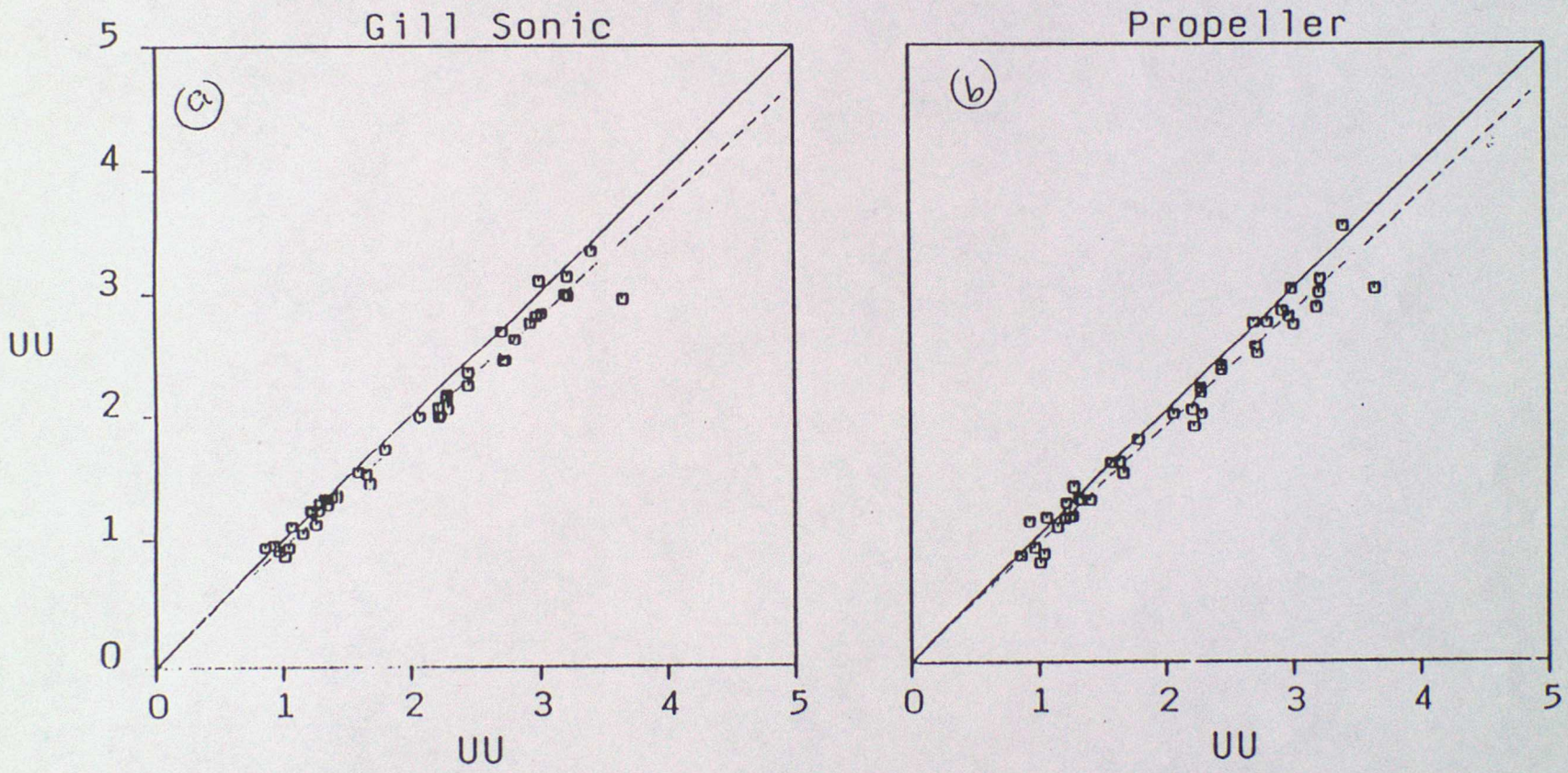

Figure 3

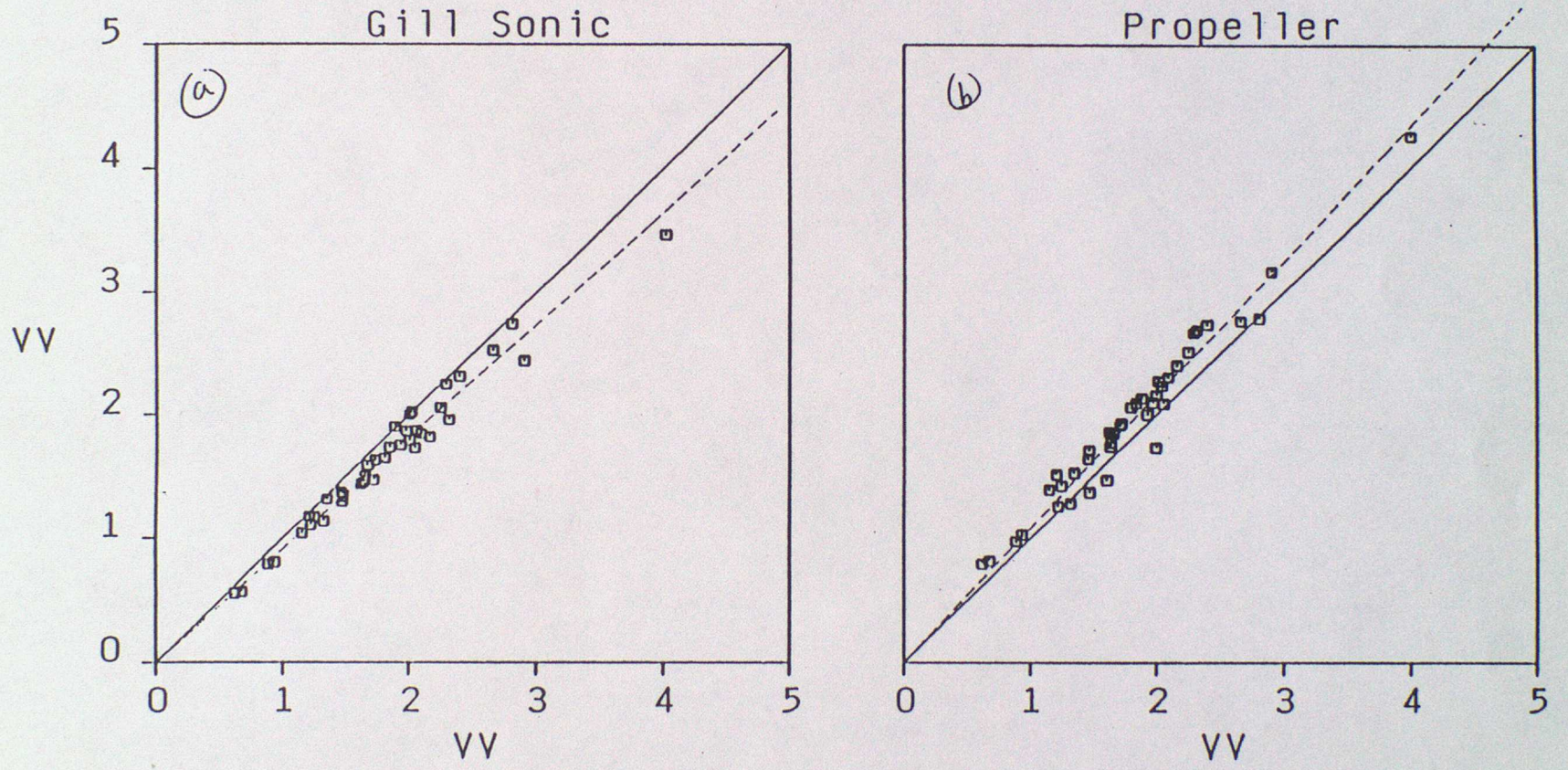

Figure 4

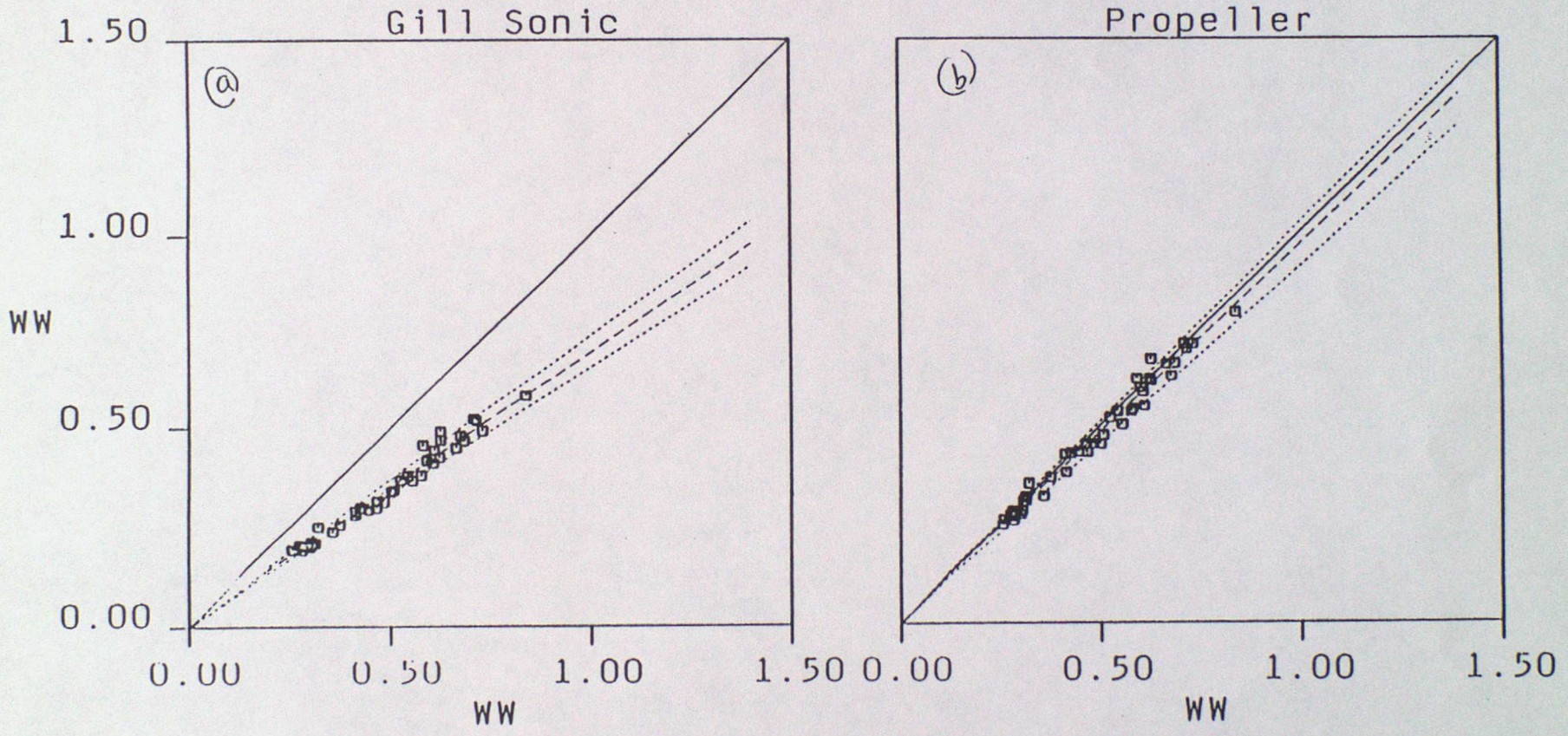
Gill Sonic
(a)
1.50
1.00
0.50
0.00
WW
0.00
0.50
1.00
1.50
WW
Propeller
(b)
0.00
0.50
1.00
1.50
WW

Figure 5

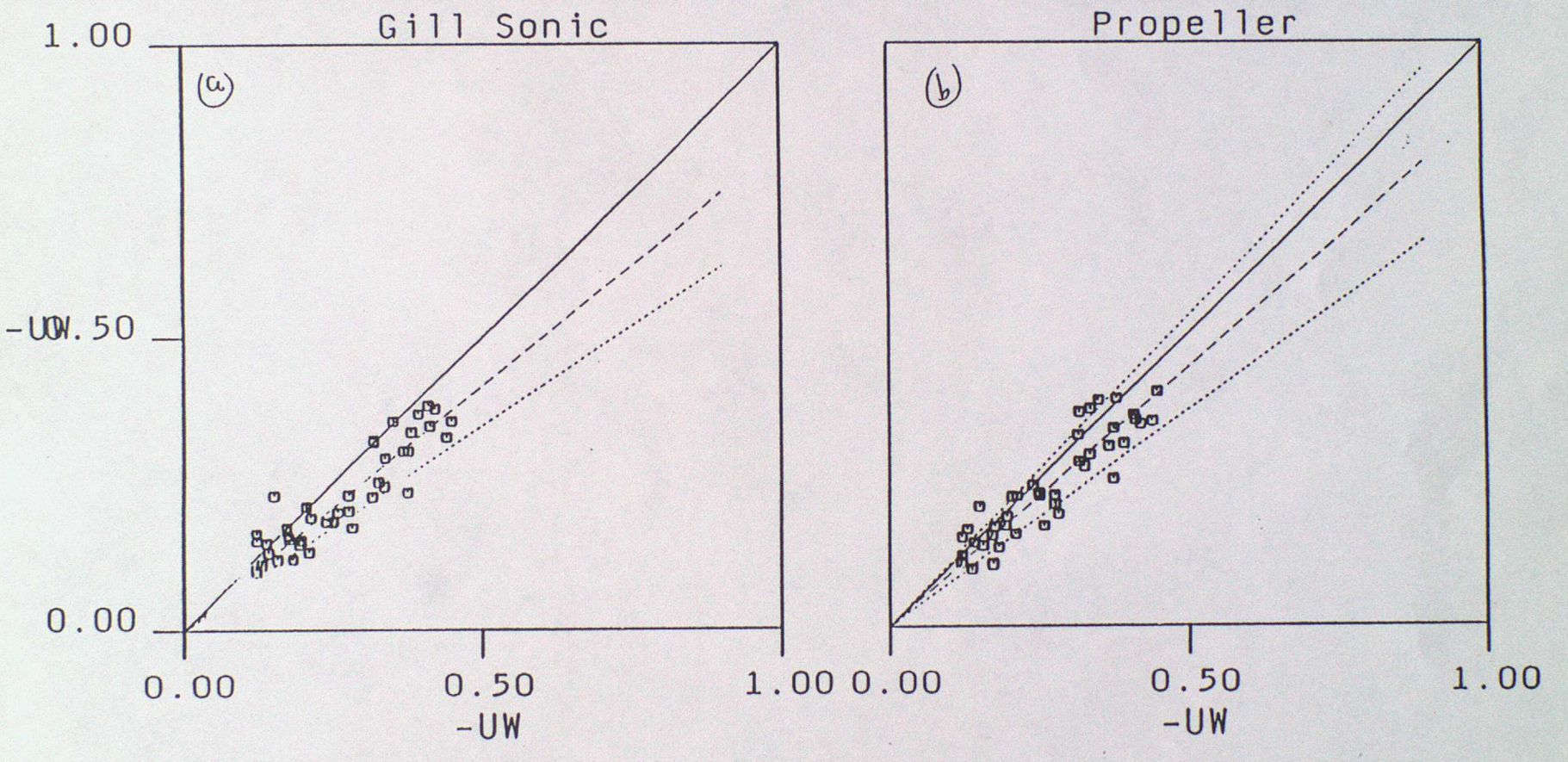
Gill Sonic
Propeller
(a)
(b)
1.00
-UW.50
0.00
0.00
0.50
1.00
-UW
0.00
0.50
1.00
-UW

Figure 6

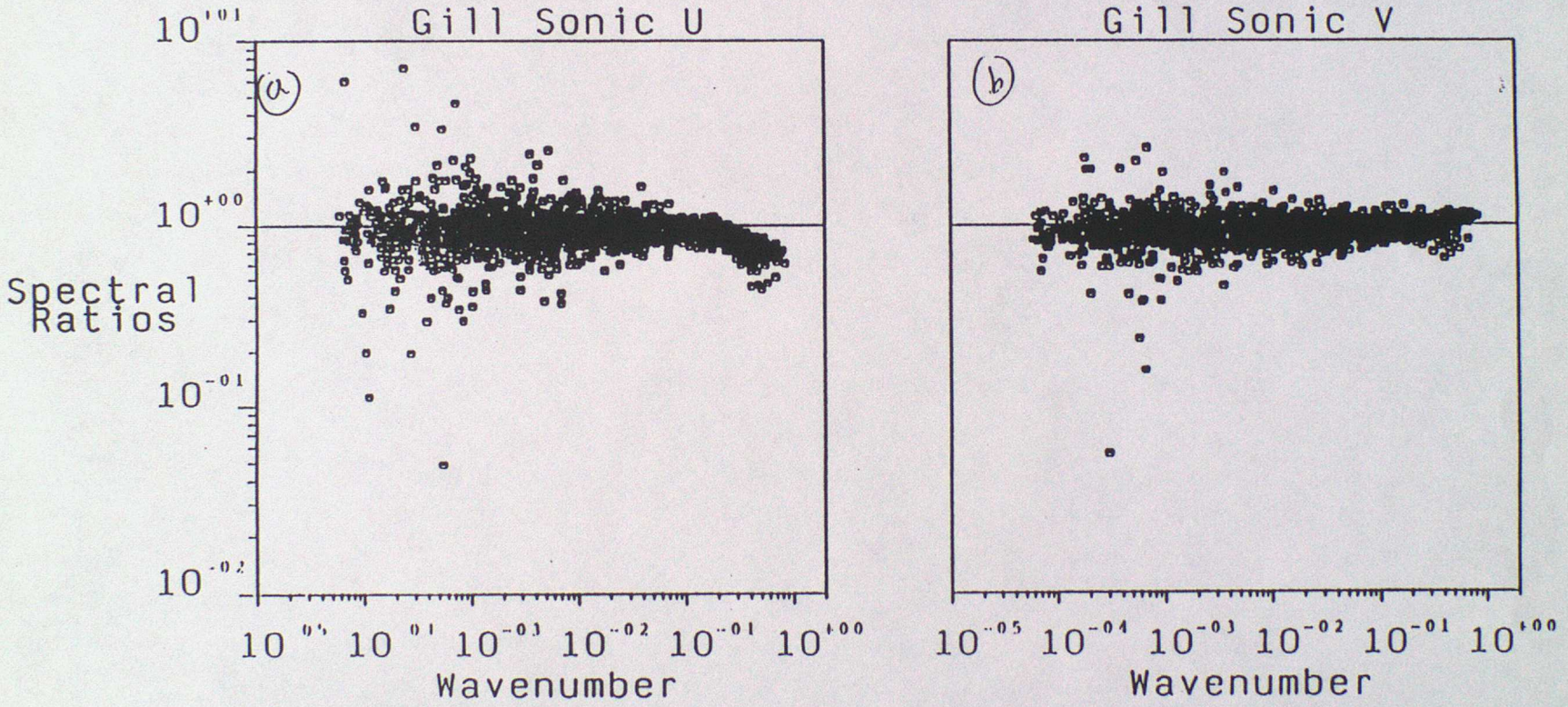
Gill Sonic U
(a)
Spectral Ratios
10^{+01}
10^{+00}
10^{-01}
10^{-02}
10^{-05} 10^{-04} 10^{-03} 10^{-02} 10^{-01} 10^{+00}
Wavenumber
Gill Sonic V
(b)
10^{-05} 10^{-04} 10^{-03} 10^{-02} 10^{-01} 10^{+00}
Wavenumber

Figure 7

Figure 8

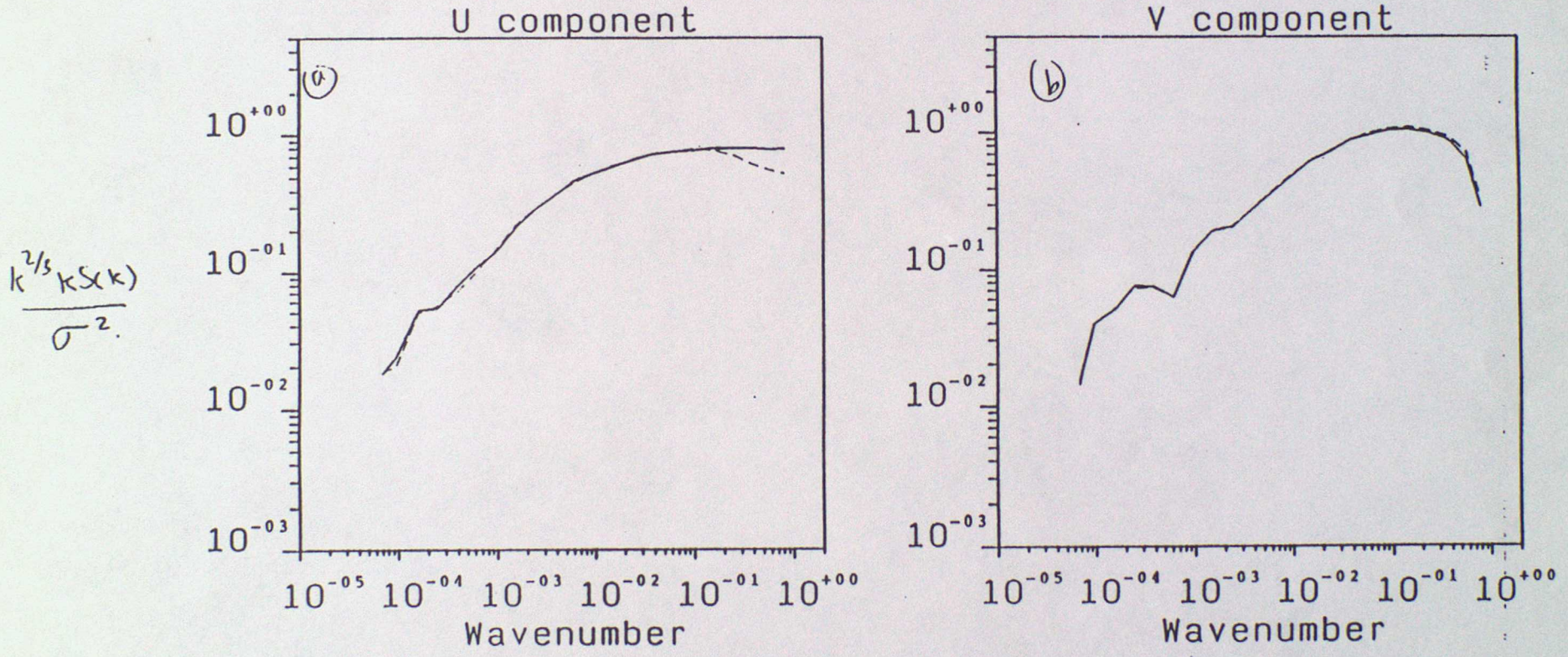
U component
V component
(a)
(b)
10^{+00}
10^{-01}
10^{-02}
10^{-03}
10^{-05} 10^{-04} 10^{-03} 10^{-02} 10^{-01} 10^{+00}
Wavenumber
$\frac{k^{2/3} kS(k)}{\sigma^2}$

Figure 9

Figure 10

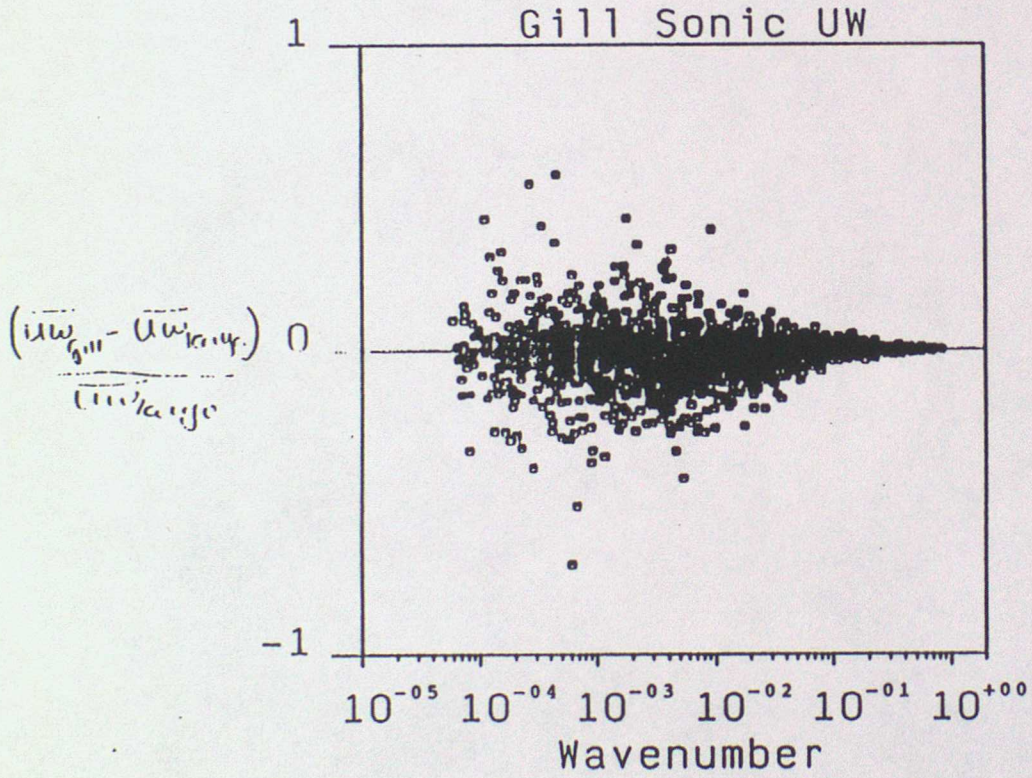

Figure 11

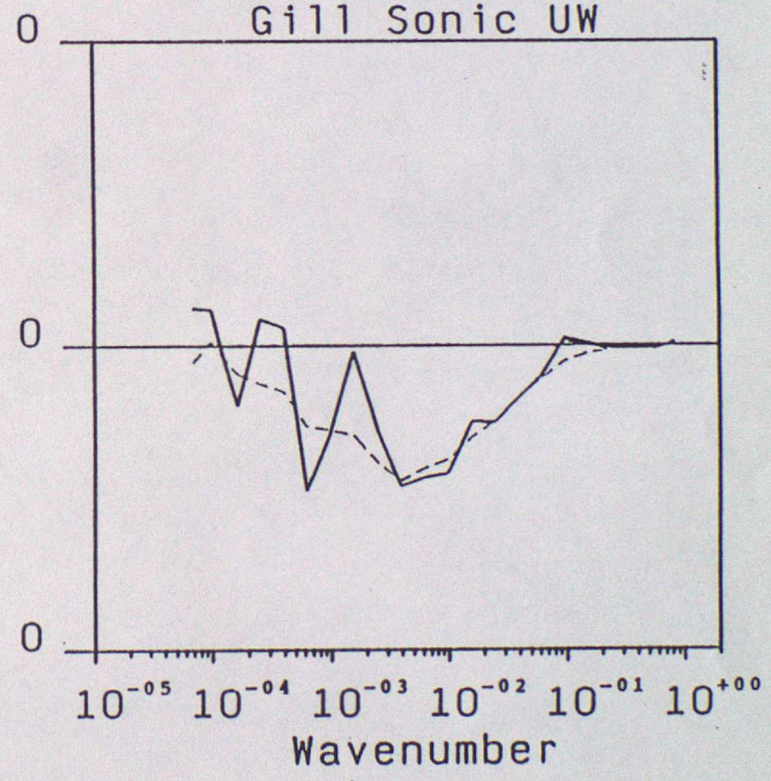

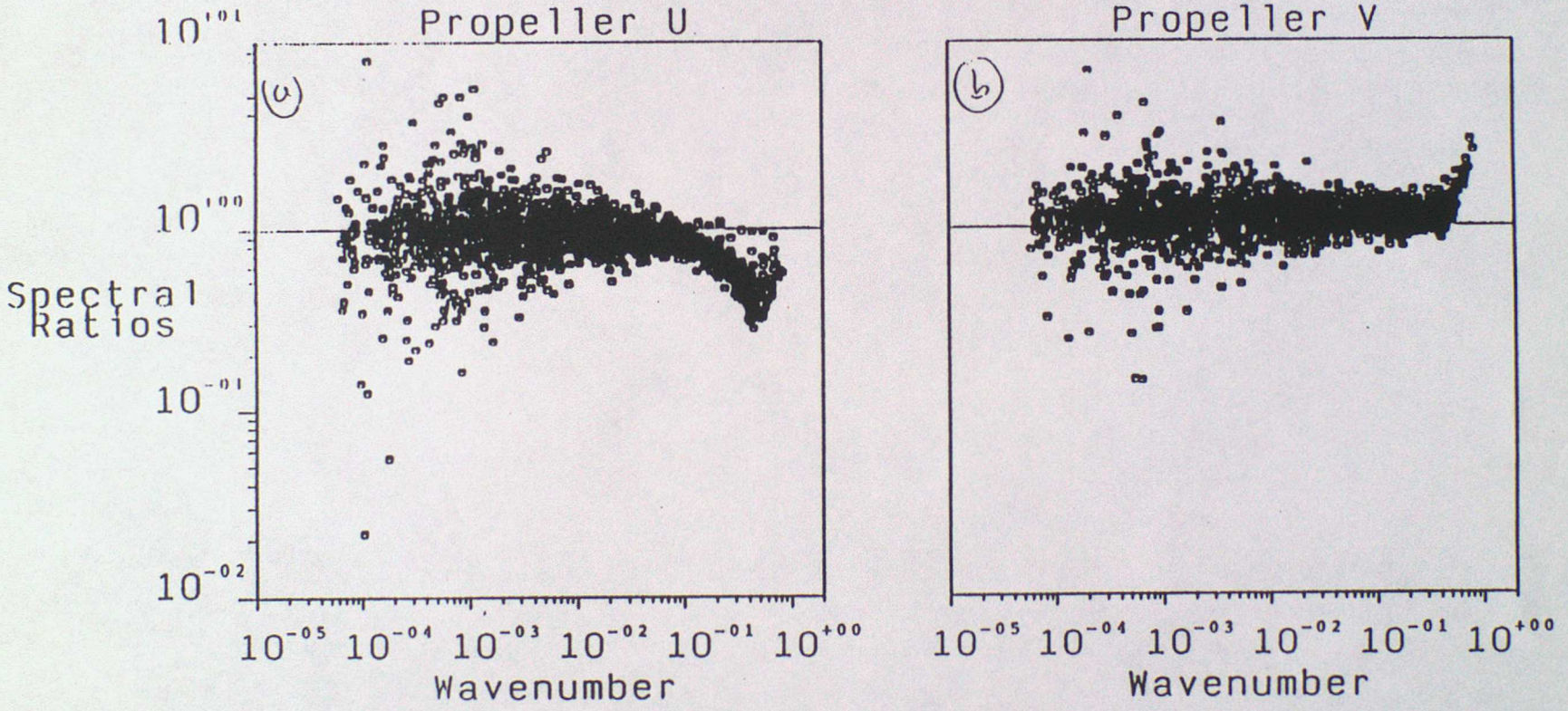
Propeller U
Propeller V
(a)
(b)
Spectral Ratios
10^{+01}
10^{+00}
10^{-01}
10^{-02}
10^{-05} 10^{-04} 10^{-03} 10^{-02} 10^{-01} 10^{+00}
Wavenumber

Figure 12

WW / UUU
10^{+01}
10^{+00}
10^{-01}
10^{-02}
10^{-03}
10^{-05} 10^{-04} 10^{-03} 10^{-02} 10^{-01} 10^{+00}
Wavenumber

Figure 13

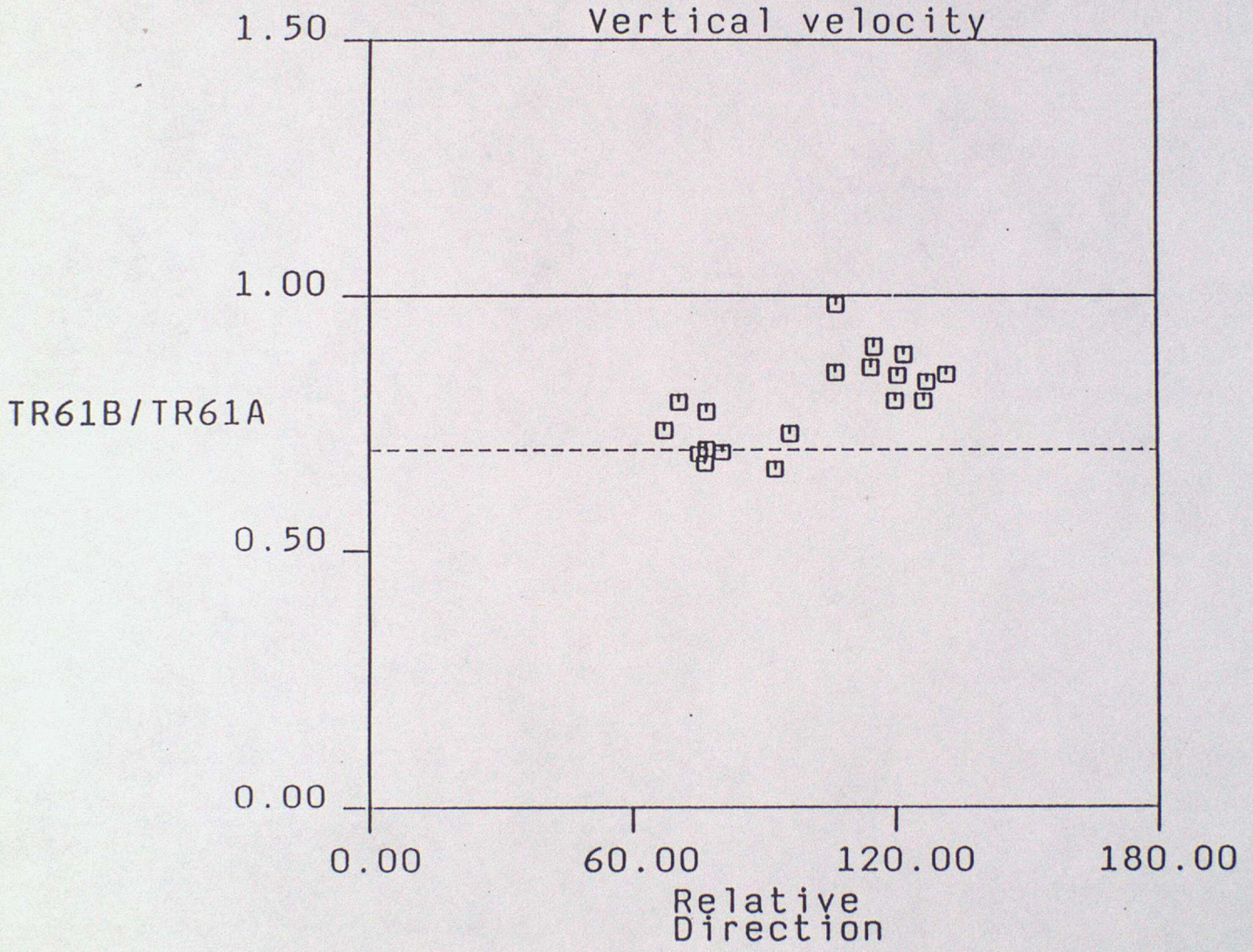
Vertical velocity
1.50
1.00
0.50
0.00
TR61B/TR61A
0.00
60.00
120.00
180.00
Relative
Direction

Figure 14